IET Microwaves, Antennas & Propagation

Research Article

IET Journals
The Institution of Engineering and Technology

Suppression of spurious harmonic responses in superconducting microstrip spiral filters using gold overlay and stagger tuning

ISSN 1751-8725
Received on 12th December 2019
Revised 19th September 2020
Accepted on 6th October 2020
E-First on 17th November 2020
doi: 10.1049/iet-map.2019.1113
www.ietdl.org

Frederick Huang[1] ✉, *Pietro Bolli*[2], *Sergio Mariotti*[3]

[1]*Department of Electronic, Electrical and Systems Engineering, University of Birmingham, Edgbaston, Birmingham, B15 2TT, UK*
[2]*Arcetri Astrophysical Observatory, National Institute for Astrophysics (INAF), Largo E. Fermi 5, Florence, Italy*
[3]*Institute of Radio Astronomy, National Institute for Astrophysics (INAF), via P. Gobetti 101, Bologna, Italy*
✉ *E-mail: f.huang@bham.ac.uk*

Abstract: The higher order resonances of microwave superconducting filters with spiral resonators were suppressed, giving a very wide stop-band. In one filter spirals were modified to have equal fundamental resonances, but different higher order resonances, by adding stubs and using non-uniform line width. The higher resonances were reduced to −39 dB, in a stop band up to 4.3 times the pass band centre. In another filter, parasitic resistive resonators were added, suppressing the responses to −57 dB. The resistance is provided by patterning the 200 nm gold overlay already required for the external contacts. The increase in pass band loss is not measurable. Measurements of a single spiral resonator with a gold-YBCO bi-layer (200 and 600 nm respectively) suggest that the resistivity of the gold layer at 15 K is the order of 22 times that of bulk gold, a slight advantage for the present application. At 100 K, it is about double.

1 Introduction

Distributed element filters, including microstrip superconducting band pass filters, employ resonators with resonant frequencies f_0, $2f_0$, $3f_0$, … where f_0 forms the required pass band but the others are spurious responses. With a step-impedance resonator, the resonances are at unequal intervals; the nth resonance has a standing wave pattern with n current maxima and can be very loosely described as the nth harmonic. The higher order resonances can be suppressed with a variety of methods, best used in combination [1–4].

An existing 10th order superconductor (Yttrium Barium Copper Oxide, YBCO) filter centred at 2295 MHz with 7% bandwidth, for radio astronomy [5], already has partially suppressed higher order responses, as a by-product of other requirements. The square spirals with large spaces in the centre move the 2nd and 3rd harmonics to approximately $3f_0$ and $4f_0$. At the fundamental frequency, currents are all clockwise or all anticlockwise, whereas in the harmonics, the currents can be in both directions, reducing the magnetic field and the coupling. This is similar to using transmission zeroes [6]. Finally, the spirals are partially unwound, by differing amounts, to provide cross coupling with non-adjacent resonators; the harmonics then occur at differing frequencies, that is, they are stagger tuned, reducing the response at any one frequency [3, 4, 7].

For the present work, 2nd and 3rd harmonics were further suppressed in this filter, to allow direct comparison. Firstly, two additional stagger tuning mechanisms were explored. Stubs were inserted, similar to [4, 8, 9] in resonators other than spirals. Step impedances were also included; they were used in other types of resonators in [10, 11]. Step impedance spirals appear in [12], but with only 1½ turns, the resonators only just qualify to be called spirals; also it is for a low pass filter and furthermore not for stagger tuning.

Secondly, additional, lossy, parasitic resonators were added. Their fundamental resonance equals the second or third harmonics of the main resonators, damping the response, similar to the mechanical tuned mass dampers in car engines and tall narrow buildings [13]. They are particularly applicable as they avoid damping the main pass band. Previously, the parasitic resonators were copper on Duroid® [14] attached to the roof of the filter enclosure, with the main resonators superconducting, or in branch lines [2] with copper main resonators. In the present work, they are gold-YBCO bi-layers (200 and 600 nm respectively), while the main resonators have only the YBCO film. The gold film already exists to provide good contact with the input and output, hitherto grossly underutilised because only a very small area near input and output was metallised. No additional processing is required. The gold thickness is fixed by the contact requirements, and the design effort concentrates around the choice of resonators. Both spiral-in-spiral-out (SISO) resonators and meander-line/interdigital capacitor (IDC) resonators were used. Even though the YBCO under-layer cannot be removed, the very narrow spurious peaks in a stagger-tuned filter are effectively suppressed; the suppression mechanisms complement each other well. Thus several suppression mechanisms were explored, instead of extracting optimum performance from one of them. Superconducting filters have previously had harmonics suppressed in [14, 15].

Stubs and step impedances are first presented, with simulated data. The sheet resistance of a gold-YBCO film is discussed, with experimental data. The parasitic resonators are described. Finally three filters are designed and tested.

Approximate analytic equations for spirals are discussed in [16], but mutual inductance between spiral turns, and capacitance between non-adjacent turns, are not addressed in detail, so results may be unsuited to some spirals. Also, ground planes and coupling between spirals are not relevant to the application described but are needed in the present work. Thus the design of the present filters depends on qualitative knowledge and simulations, as far as possible using resonators singly or in pairs, which take seconds or minutes, before addressing the whole filter, which takes hours (using SONNET® [17] 'edge mesh') or days (with 'fine mesh') with a 4-core 3.2 GHz computer with 8 GB of RAM. Because of the stagger tuning, there are up to 10 separate second harmonic peaks. The resonator (or resonators) responsible for each peak are found by observing simulations of current density or by simulating each resonator separately, together with the frequency shift with respect to the chosen adjustable resonator dimension. When two peaks are close together but not coincident, the estimate (18) in [4] suggests that doubling their separation reduces their amplitudes by 6 dB. Finally, the pass band is readjusted, using the design procedure from [5]. Hence the design is iterative but not a blind optimisation.

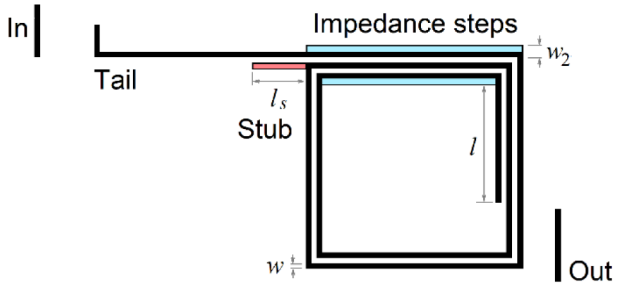

Fig. 1 *Spiral resonator, with modifications*

Table 1 Shift in second harmonic frequency of stubs and step impedances

Stubs			Impedance steps		
l_s (mm)	l (mm)	f_2 (MHz)	w_2-w (mm)	l (mm)	f_2 (MHz)
0.0	1.32	6632	0.00	1.09	6732
0.1	1.305	6599	0.015	0.925	6799
0.2	1.29	6562	0.05	0.61	6914
0.5	1.235	6451	0.06	0.53	6939

Tail length = 2.2 mm. Step size is w_2-w.

Measured values of gold film resistivity only became available when the filters were also measured, so the design procedure is illustrated with a re-run using the measured gold-film data. The original data based on bulk gold resistivity [18] at 20 K gave suppression which was a few dB poorer than the final version, but is otherwise very similar.

2 Stagger tuning with stubs and step impedances

Stubs (red) and impedance steps (blue) are shown in Fig. 1. The original resonator is a 2×2 mm^2 spiral, partially unwound forming a 2.2 mm tail. The 0.5 mm thick Magnesium Oxide (MGO) substrate has dielectric constant $\varepsilon_r = 9.65$, and the line width is $w =$ 0.05 mm.

The stub is placed at the point where the outermost turn joins the next turn; if the spiral is unwound and straightened, the stub is as close as possible to the centre, without changing the original spiral. At the fundamental, it is close to a voltage minimum so the resonance is only slightly shifted by the stub. At the second harmonic, the voltage maximum results in a larger shift. In simulations, l is adjusted to keep the same fundamental, and the 2nd harmonic frequency is given in Table 1. The coupling coefficient is assumed to be unchanged, and like the fundamental, the third harmonic is not much affected.

The impedance steps result from step changes in the track width (Fig. 1). The regions of increased width are chosen so that coupling between resonators is not greatly affected. In this paper w_2 is chosen to optimise the second harmonic, and the third harmonic is re-adjusted by other means, instead of optimising two harmonics simultaneously. Simulations (Table 1) show relatively coarse tuning for a given w_2-w. Also, taking the top row of the table (no stub and no step) shows that the second harmonic shifts by 100 MHz for a 0.23 mm change in l.

3 Sheet resistance of gold-YBCO bi-layers

Since the focus of this paper is on filters, limited attention has been given to the gold film. Furthermore its main purpose is the external contacts; perhaps the only flexibility to optimise resonance suppression is to vary the thickness between about 100 and 500 nm. The normal skin effect is considered. It may be strongly influenced by the proximity effect [19, 20], where the gold and YBCO affect each other's properties. The anomalous skin effect [21, 22], is ignored, and therefore not eliminated.

The surface impedance of a thin layer of gold on YBCO can be written as [20, 23],

$$\frac{Z_s}{Z_\infty} = \frac{1 + [((1-j)/2)](\delta/\lambda)\tanh[((1+j)/\delta)t]}{[((1-j)/2)](\delta/\lambda) + \tanh[((1+j)/\delta)t]} \quad (1)$$

where: Z_s is the surface impedance of the bi-layer; $Z_\infty = (1+j)\sqrt{\rho\pi\mu_0 f}$, is the surface impedance of a thick layer of gold, greatly exceeding the skin depth δ of gold; $\lambda = 150$ nm is the penetration depth of the underlying YBCO [24, 25]; $t = 200$ nm, the thickness of the gold layer; and ρ is the resistivity of gold.

The YBCO thickness is four penetration depths, where the magnetic field has decreased to e^{-4} or 2% of its original value, so it can be taken to be infinite. If the gold resistivity is low, the current is mainly in the gold, making the effect of finite YBCO thickness even smaller. If gold resistivity is very high, the main effect of the finite YBCO thickness is a small change of its inductance, which changes the amount of current which bypasses the gold.

In simulations, the microstrip has a resistive gold/YBCO top surface with resistance $R_s = \mathrm{Re}(Z_s)$ and a downwards-facing plain YBCO surface (touching the substrate), taken to be lossless (Fig. 2*a*), joined by vias at regular intervals. They have approximately equal currents, as confirmed by comparing with a hypothetical case with the resistive layer R_s at the bottom and the lossless layer on top, and finding losses to be approximately equal. Thus the same attenuation occurs if top and bottom surfaces both have a resistance of $R_s/2$, or if combined as a thin layer of resistance $R_{\mathrm{equiv}} = R_s/4$. This reduces computation time in subsequent simulations. In Method of Moment (MOM) calculations, the strip is divided into sub-cells, each usually with a constant current distribution. This does not fully account for the current crowding at the edges (with sub-cell size 0.0025 mm). Meanwhile the real strip has finite thickness (800 nm) with current also flowing in the side-walls. Comparing data in [26] with [27] suggests that the surface resistance may be as much as 20% less than estimated, but [27] was not yet available at the time of this work; also, it does not specifically consider two different materials in combination.

Measurements of the spiral (Fig. 2*b*) are shown in Fig. 2*c* for 15 K, with gold placed on the main resonator and with no adjoining parasitic resonators, nor step width changes, but accidentally including a stub (of no consequence). The assembly procedure is the same as the main experiments in Section 6. Processing of the measured data is described in the appendix.

For very low resistivity, at the left-hand side of Fig. 2*c*, the current is almost all in the gold, because the superconducting path creates a greater magnetic field (in the gold), that is, more inductance; this is the skin-effect. At very high gold resistivity, current is diverted to the YBCO, reducing the loss. Except for a small discrepancy at 16.3 GHz (the measured point almost

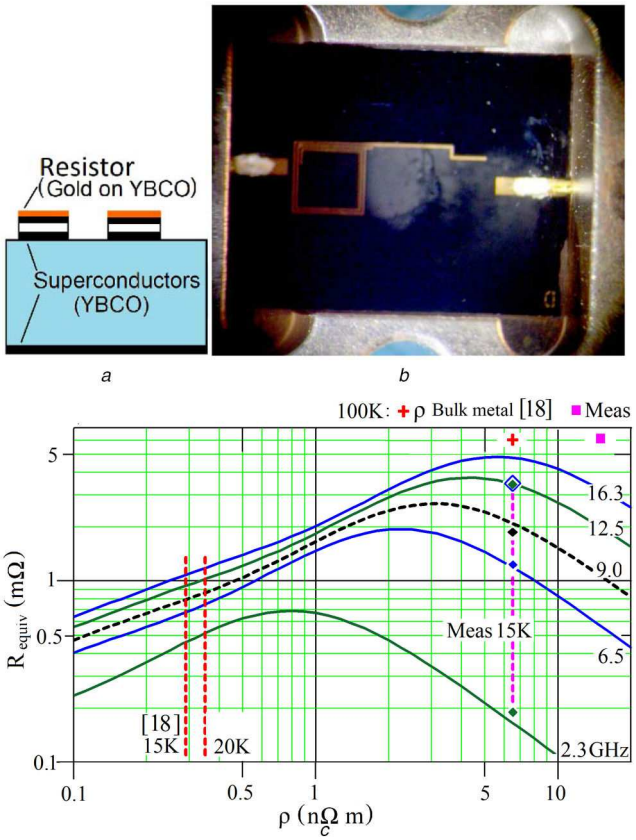

Fig. 2 *Equivalent sheet resistance of a combined gold/YBCO bilayer, 200 and 600 nm thick*

(a) Model for combined layers, ***(b)*** Measured resonator. Contrast is digitally enhanced, ***(c)*** Equivalent sheet resistance from (1) as a function of gold resistivity; bulk gold [18] and measured data are compared

coincides with 12.5 GHz), the values fit the calculated ones well if an effective gold resistivity is taken to be about 22 times higher than bulk gold at 15 K [18], or perhaps more, from the abovementioned possible 20% error, and the negative gradient. In a comparison, the straight coplanar lines 'S1' and 'S2' from [28] were simulated (using SONNET), adjusting R_{equiv} to match the reported loss; R_{equiv} is estimated as 2.5×10^{-3} and 5.6×10^{-3} ohms at 10 GHz, somewhat larger than here, because of the different thicknesses of YBCO (300 nm) and gold (also 300 nm). Other works [29, 30], report even higher gold resistivity, probably because of the deposition techniques then available, together with different substrates and temperatures.

At 60 K, the measured values of R_{equiv} (2.3, 6.5 and 9 GHz only) are very similar to 15 K and therefore not plotted in Fig. 2. The increase in superconducting resistance in the lower microstrip surface may obscure a decrease in Re(Z_s), that is, a small increase in ρ (resulting from the negative gradient). At 100 K, where YBCO was assumed to be a perfect insulator and the 200 nm gold thickness is much smaller than the skin depth, calculations assume that current density does not vary with depth. Averaging values at 6.5 and 9 GHz, gold resistivity was estimated as about 15×10^{-9} Ωm, approximately double that of bulk gold at this temperature [18]. (The vertical scale is not relevant for 100 K.)

The values of R_{equiv} extracted for subsequent comparisons with filter measurements are 0.19, 1.23 and 1.85 mΩ for 2.3, 6.5 and 9.0 GHz respectively. Compared with the estimates based on bulk gold (15 K), they are advantageous because the filters require low additional loss at the fundamental resonance and as much loss as possible for the others. Also, for the present filter, nearly the maximum sheet resistance of the 200 nm gold layer can be utilised. In a sense, the data are ill-conditioned with a small error in measured R_{equiv} leading to a large error in the estimate of ρ, but this is not relevant because R_{equiv}, is to be used directly in design. Indeed the reverse relationship is favourable in that a large error in ρ can be tolerated, amounting to a massive error margin.

The salient characteristic of lower-than-predicted R_{equiv} for 2.3 GHz and higher values for other frequencies does not eliminate other explanations. Re-running Fig. 2*c* for $t = 150$ and 250 nm, the same pattern is obtained, with new values of ρ; the same may apply with the anomalous skin effect. Thus the outcome is to show that this characteristic is reasonable and not to distinguish between the normal and anomalous skin effects.

4 Parasitic resonators

The 2nd harmonic of a main resonator, a grey spiral in Fig. 3, can be loaded with the fundamental resonance of a lossy parasitic resonator, between 6400 and 6900 MHz. A further parasitic resonator suppresses the 3rd harmonic, between 8500 and 11,000 MHz. One design is a meander line joined to an IDC (Figs. 3*a* and *b*); another is the spiral-in-spiral-out resonator (SISO) [31, 32] (Fig. 3*c*). In the meander, adjacent sections have opposite currents, whose magnetic fields cancel as distance from the resonator is increased, resulting in a larger resistance to inductance ratio, that is lower quality factor. The same applies for the SISO. This is necessary because of the small loss of the gold.

In simulations with one main resonator and one parasitic resonator, also with input and output similar to Fig. 1, SONNET 'edge mesh' and a cell size of 0.005 mm were used. Typical responses are given in Fig. 4. With one resonator only (purple), the solitary peak has only superconductor losses plus input and output loading, but when the parasitic resonator is added the losses due to the gold dominate and furthermore it is split into two maxima. Increasing the gold film resistance would suppress responses further, until the current in the second resonator starts to decline [14], but this optimum loss is not sought because the gold thickness is determinied by the requirements of the external contacts. Increasing the coupling coefficient also reduces the response by separating the peaks further, but only gradually, and at the expense of a slightly higher passband loss. The second harmonic response could still have been suppressed further, since the peaks have so far been spread only over a narrow band, 6400–6900 MHz.

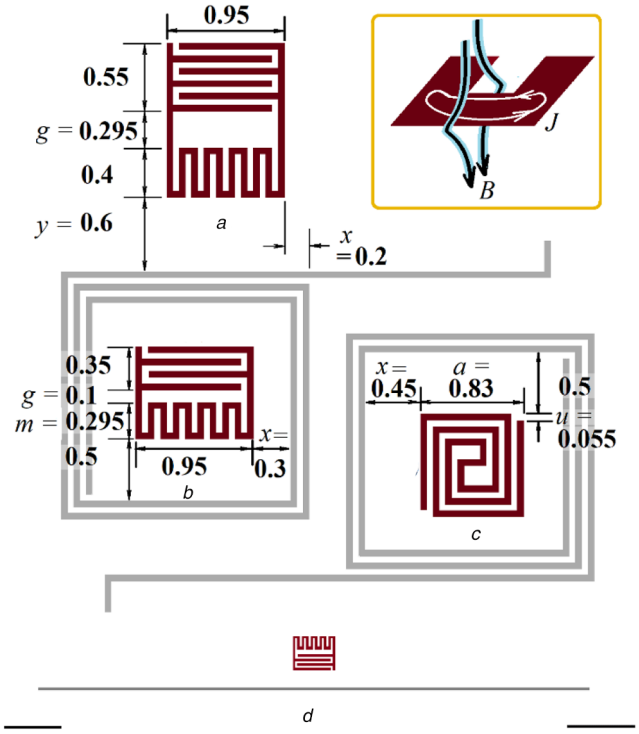

Fig. 3 *Parasitic resonators (dark brown) coupled with the main resonators (light grey). Dimensions in mm*

(a) Meander line/interdigital capacitor (IDC) resonator for second harmonic, ***(b)*** Meander line/IDC resonator for 3rd harmonic, ***(c)*** Spiral-in-spiral-out resonator (SISO) for 3rd harmonic, ***(d)*** Parasitic resonator and straight microstrip

Inset: current pattern resulting from an externally applied magnetic field

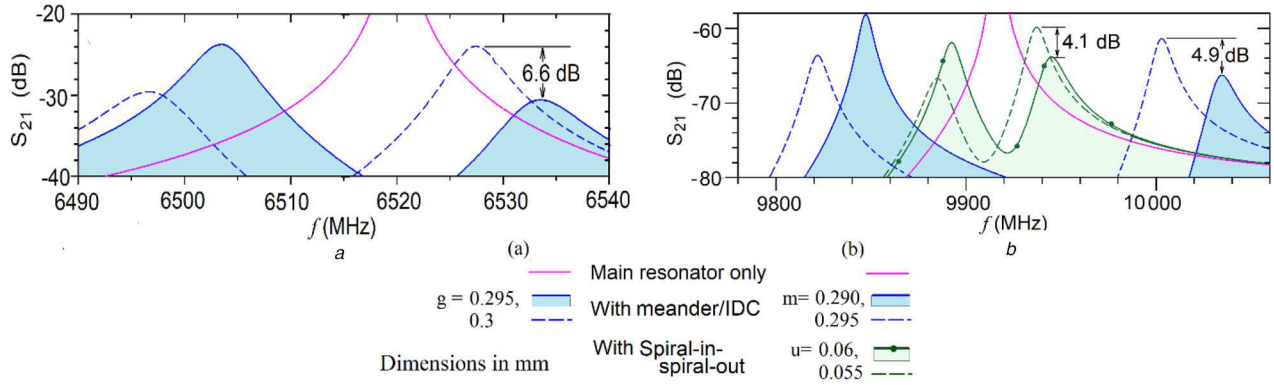

Fig. 4 *Frequency staggering and attenuation from the parasitic resonators. Fixed dimensions are given in Fig. 3*

(a) Second harmonic, ***(b)*** Third harmonic

The meander/IDC and SISO resonators also have significantly different levels of coupling to the main resonators, so that the separation between the two peaks is different, providing the stagger tuning at the third harmonic, since the mechanisms described in Section 2 are already allocated to the 2nd harmonic.

To assist the iterative fine tuning procedure, the reduction of the higher peak for a 0.005 mm adjustment in one of the dimensions is given. Since the second harmonic resonators are stagger tuned, each maximum corresponds to one particular resonator; the corresponding parasitic element is adjusted. The initial design requires data on parasitic resonator dimensions for a given resonance frequency. These were found from simulations, and are given in Fig. 5. The third harmonic frequency range is larger and requires tuning two dimensions, for coarse and fine tuning. For even finer tuning of the meander resonators, the length of one of the capacitor fingers could have been varied instead.

The estimated passband quality factor associated with the parasitic resonator (Fig. 3*a*) is 2×10^7, much higher than even the superconductor resonator, because the parasitic resonator is not resonant, and only loads the main resonator slightly. The 3rd harmonic resonators have a Q factor of about 5×10^5, much smaller but still far better than the superconductor. Here, the loss is mainly due to the eddy current induced by the external field from the main resonator, as illustrated in the inset of Fig. 3. Currents are opposite on the two sides of a track, and need the track to have more than one simulation cell.

The coupling mechanisms are difficult to evaluate when one resonator is completely enclosed by another; both electrical and magnetic coupling arise from all sides. Some insight can be obtained with a one-wavelenth (instead of a half-wavelength) straight microstrip. It has a voltage maximum at the centre, and current maxima at the ¼ wavelength points. Placing the meander close to these points (Fig. 3*d*) it was found that the meander resonator coupling is mainly magnetic, as explained by the inhomogenous dielectric (MGO and vacuum), where the self-capacitance is mainly in the MGO, but the mutual capacitance is mainly associated with the vacuum and therefore small. Even when the capacitor fingers are closest to the straight line, the magnetic coupling is typically twice as large. For the SISO, adjacent turns have currents in opposite directions and weak magnetic fields, so the electrical coupling was found to dominate.

An alternative position for the 3rd hamonic suppressor is near a tail, in the space occupied by the inset of Fig. 3. The flexibility of distance from the main resonator makes coupling coefficient more

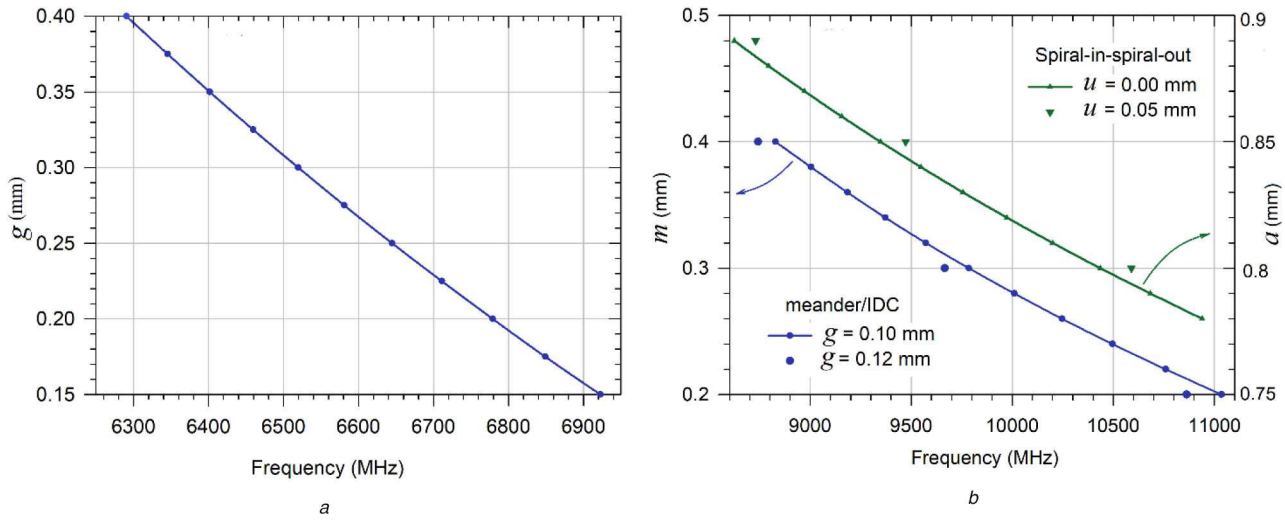

Fig. 5 *Frequency dependence of parasitic resonators (dimensions are defined in Fig. 3)*
(a) Second harmonic, ***(b)*** Third harmonic

adjustable. The increase in pass band loss is even lower than the 2nd harmonic resonator. The initial belief of unwanted coupling with another main resonator (Fig. 3) was unfounded, being given in simulations to be only about a tenth as large.

5 Filter design

The filter [5] was modified to reject harmonics. The original design is similar to Fig. 6, but with no Gold/YBCO resonators, and a uniform line width of 0.05 mm except at the input and output. The dimension *l* (Fig. 1) in all the resonators was shortened slightly by 0.06 mm, to shift the passband upwards by 7.2 MHz and make it more central with respect to the original specification. The internal box size was increased slightly to $30 \times 10 \times 6.5$ mm^3 to accommodate the extra resonators. In three new filters, suppression mechanisms were progressively added, for better and better suppression.

In filter 1, stubs and impedance steps were included to stagger tune the 2nd harmonic resonances, using the data from Section 2. With the stagger tuning, each peak is associated with only one resonator, and is adjusted independently using the data in previous sections. The use of impedance steps also spaces out the 3rd harmonics, but the original aim was only to demonstrate 2nd harmonic suppression. SONNET simulations used a cell size of 0.0025 mm.

Passband characteristics were fine-tuned by varying *l* and the gaps between resonators, using the iterative design procedure [5]. Because the addition of stubs and steps above was already accompanied by an adjustment of *l,* the fine-tuning was at most 0.01 mm, 4 times the cell size, but usually much less. The design procedure does not allow for non-symmetric filters, but only small differences had been introduced between resonators *n* and 11-*n* ($n = 1 \ldots 5$), so in the pass band the filter remained approximately symmetrical.

For filter 2, the 2nd harmonics were reduced further using the meander/IDC resonators. The gap between main and parasitic resonators is 0.6 mm for resonators 2–9, while resonators 1 and 10 are already damped by source and load resistances, so the gap was 1 mm. The harmonic bands were simulated using a coarser, 0.005 cell size and 'edge mesh' setting. Although the stop band is the focus of the present study, an error of (for example) 1 dB is acceptable, whereas in the pass band, even 0.1 dB is very large.

For the passband evaluation, the previous 0.0025 mm cell size was retained for the main resonators, but meander/IDC resonators 1 and 10 were omitted for computational economy, since they are further away from the main resonators. The other parasitic resonators used 12.5, 25 and 12.5 µm sub-cells across the 50 µm line width. The increase in passband loss is 2×10^{-5} dB, obtained by comparing a simulation with gold loss only against the lossless case.

Finally in filter 3, the 3rd harmonic parasitic resonators were added. Both 2nd harmonic and main resonators were fine-tuned. For the pass band simulation, the 2nd harmonic parasitic resonators were omitted for computational economy, having been found to have very little effect, as above. The estimated extra loss is 1.4×10^{-3} dB. The final filter 3 is presented in Fig. 6 and the dimensions of the three filters listed in Table 2.

6 Filter measurements

Each filter was glued in a titanium box (which has a similar expansion coefficient to the MGO) silver-plated (instead of gold, for economy), with a conducting, adhesive film (Ablestick 5025) using a standard curing procedure, at 100°C for 240 min under a 100 g weight. K-connectors including glass beads and later, sliding contacts were installed following Anritsu procedures, and joined to the input and output lines with gold bond wires buried in conducting epoxy (AiT 8050LV). The wires improve reliability in case the epoxy cracks. The final filter is presented in Fig. 7. A (very rare) processing residue, which was not removable using common solvents, appeared to have no effect on filter performance, suggesting that a protective coating to guard against moisture could be applied without filter degradation.

Before installing the sliding contacts and epoxy, the filter with weak capacitive external coupling was measured, resulting in 10 sharp pass band resonances; comparing filters 1 and 3, they were intended to give the quality factor of the resonators as loaded by the YBCO/gold resonators [33]. Even with this method, it was not possible to measure the increase in pass band loss introduced by the gold layer, because it was smaller than expected (as related in Section 3), and smaller than the scatter of loss values with no gold. It only confirms that Q for the parasitic resonators is indeed very much higher than the main resonators themselves, which have a Q factor of about 60 000.

For the complete filters, ideally the band 2000–12 000 MHz should be measured in 0.2 MHz steps; the available network analyser would require 50 000 measurement points in about 33 frequency ranges of 1601 points each. However, previous experience indicates that the harmonic frequencies tend to be accurately simulated, with only their amplitudes in question. The measurements therefore concentrate on the 2nd and 3rd harmonic bands. The first band is 6400–6900 MHz, in 0.3125 MHz steps, later combined with a further measurement, 6850–7250 MHz because of a peak near the edge of the original band. Similarly, 8800–12,000 MHz was covered in 5 bands, with 0.4 MHz steps, later extended downwards to 8700 MHz. Comments on sparse sampling are given in the appendix. SOLT calibration at room temperature avoided the many cooling cycles required to measure each calibration standard at low temperature. The harmonics are pessimistic by an estimated 0.5 dB as a result. The rest of the stop

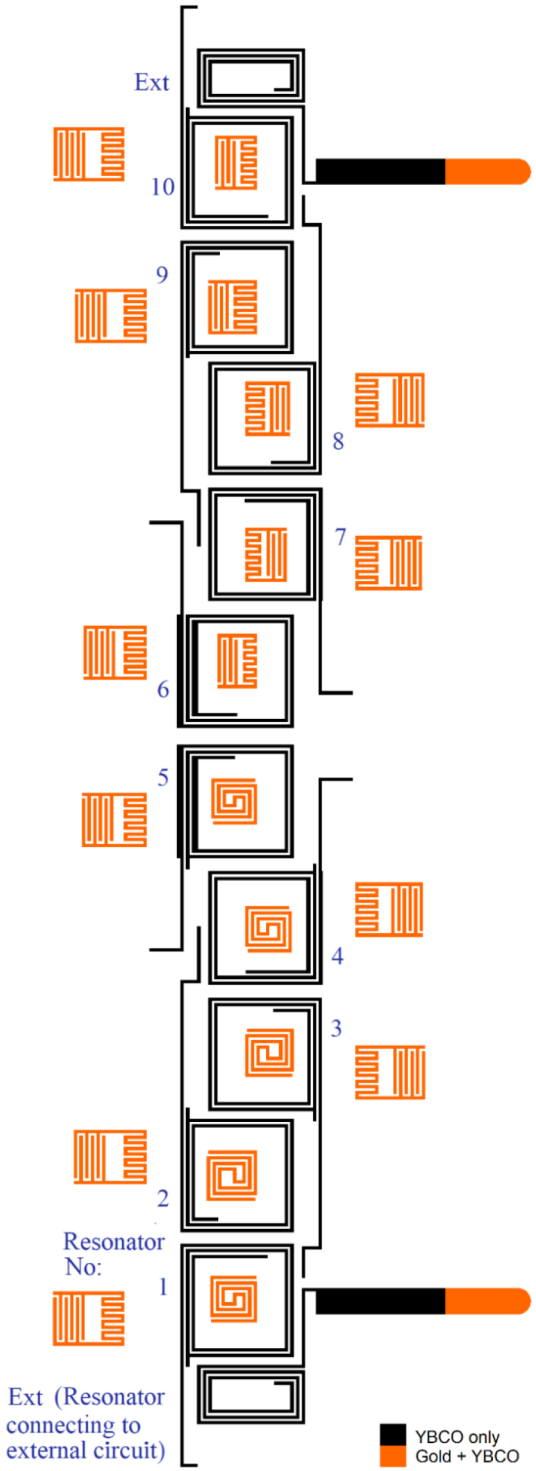

Fig. 6 *Layout of filter 3 (Filters 1 and 2 have slightly different dimensions; also filter 1 has no gold/YBCO resonators while filter 2 has only the gold/YBCO resonators outside the main resonators). Overall length is 25.84 mm, less than a half wavelength for this substrate*

band could also have used room-temperature calibration, but it was done with the pass band, with sparse sampling and TRL calibration at low temperature, since the pass band requires greater accuracy.

Filter 1 is compared with [5] in Fig. 8*a* and Table 3; with variable shades to avoid obscuring the other curves. The 2nd harmonic is improved by 33 dB. The 3rd harmonic was not considered in the design but is also improved by the stagger tuning, with some of the peaks shifted to 10,200 MHz and 10 500 MHz, away from the others. In Fig. 8*b*, filter 2 has its second harmonic suppressed by a further 17 dB; only this band is shown since no modifications were directed at the third harmonic. Returning to Table 3 and the stop band up to 11 400 MHz, filter 3 is a further improvement of at least 19 dB over filter 1. Data smoothing is described in the appendix.

Some measured data from the literature are compared in Table 4. The criterion that f_{max}/f_0 (Stop-band limit/passband centre) be at least 3.0 means that at least the 2nd and 3rd harmonics must be suppressed or shifted to the right. The present work is represented by filter 3, with two levels of suppression depending on the stop band width required. Some of the data are approximate because they have been read off the published graphs, and in [34] f_{max} is taken to be the highest frequency plotted. Also, [35] claims only −45 dB, apparently a pessimistic, rounded value.

Compared with [5], the larger box allows a spurious direct coupling between the input and output spirals, so the background level between 10 000 and 12 000 MHz increases by about 20 dB, confirmed by simulations with only the input and output spirals in the box. The larger box might not have been necessary, since the

Table 2 Resonator dimensions (mm) for the 3 filters

resonator no. (n)	Gap (n,n + 1)	Main resonator				2nd harmonic Meander		3rd harmonic		
		l	tail	w_2-w	l_s	y	g			
Filters 1 and 2										
ext	0.1450	0.2900	--	--	--	--	--	—	—	—
1	0.2100	1.2900	2.20	--	0.17	1.0	0.295	—	—	—
2	0.1425	0.4175	3.70	--	0.20	0.6	0.325	—	—	—
3	0.2300	0.6050	3.25	--	0.18	0.6	0.270	—	—	—
4	0.2350	1.0750	2.20	0.015	0.13	0.6	0.230	—	—	—
5	0.3050	0.6475	2.20	0.060	0.20	0.6	0.185	—	—	—
6	0.2350	0.6875	2.20	0.060	--	0.6	0.155	—	—	—
7	0.2300	1.0950	2.20	0.015	--	0.6	0.210	—	—	—
8	0.1425	0.6400	3.25	--	--	0.6	0.260	—	—	—
9	0.2100	0.4475	3.70	--	0.07	0.6	0.315	—	—	—
10	0.1450	1.3000	2.20	--	0.15	1.0	0.285	—	—	—
ext	--	0.2900	--	--	--	--	--	—	—	—
Filter 3								Spiral-in-spiral-out		
								x	a	u
ext	0.1425	0.2900	--	--	--	--	--	--	--	--
1	0.2075	1.2900	2.20	--	0.17	1.0	0.300	0.450	0.820	0.015
2	0.1425	0.4125	3.70	--	0.20	0.6	0.335	0.415	0.880	0.030
3	0.2300	0.6075	3.25	--	0.18	0.6	0.275	0.450	0.850	0.025
4	0.2375	1.0775	2.20	0.015	0.13	0.6	0.240	0.460	0.815	0.050
5	0.3075	0.6475	2.20	0.060	0.20	0.6	0.195	0.450	0.800	0.030
								Meander		
								x	m	g
6	0.2375	0.6875	2.20	0.060	--	0.6	0.165	0.2000	0.240	0.100
7	0.2300	1.0975	2.20	0.015	--	0.6	0.220	0.1975	0.275	0.100
8	0.1425	0.6425	3.25	--	--	0.6	0.265	0.2025	0.340	0.100
9	0.2075	0.4425	3.70	--	0.07	0.6	0.320	0.2000	0.405	0.095
10	0.1425	1.3000	2.20	--	0.15	1.0	0.290	0.1975	0.285	0.095
ext	--	0.2900	--	--	--	--	--	--	--	--

Parameters are defined and constant values given in Fig. 3.

'Ext' Resonators are the coupling spirals connecting to the external circuit.

The variables *tail*, w_2-w and l_s, are identical for all 3 filters, and y for filters 2 and 3.

For filter 1, the 2nd harmonic meander resonators do not exist so those dimensions are not relevant.

The variable x was intended to keep the fundamental frequency constant, but varying x is probably unnecessary.

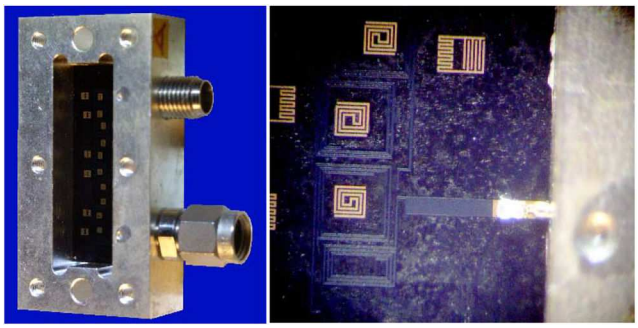

Fig. 7 *Photograph of filter 3, and enlargement. In the enlargement, contrast is digitally enhanced to show black microstrip on black background, which also greatly exaggerates a processing residue*

required gap between a spiral and the box wall is not known. Fig. 8*c* shows the pass band of the filters; the pass band has 0.15 dB maximum ripple, while the measured maximum S_{11} is −15 dB. The response has shifted upwards by 16 MHz instead of the planned 7.2 MHz, but with very little change in shape. Thus the cause is one that affects all resonators approximately equally, such as a wafer-to-wafer variability in substrate permittivity. A higher order filter would not necessarily be more prone to error and its steeper transition region skirts would allow a greater error margin. Alternatively, a lower box roof could act as a shared tuning screw, but not for these filters where the pass band is already too high. In extreme necessity, two to four filters, each with a slightly different centre frequency, can be fabricated on each two-inch wafer, and the best filter chosen.

Harmonic S_{21} peaks have been suppressed without attempting to flatten S_{11} and S_{22}, and for filter 3, S_{11} and S_{22} have notches of −39 dB and −25 dB at 10.01 and 9.96 GHz respectively, due to absorption by the parasitic resonators 1 and 10. Probably because they are already loaded by input and output, the gold overlay can be omitted; simulations show that suppression degrades only by about 2 dB, while those notches are flattened to −2.5 dB or better, but not back to −0.7 dB as offered by filter 1.

Responses in the 2nd and 3rd harmonic bands of filters 1 and 3 are compared with the simulated curves in Figs. 9 and 10. They show good agreement as to the resonance frequencies, but

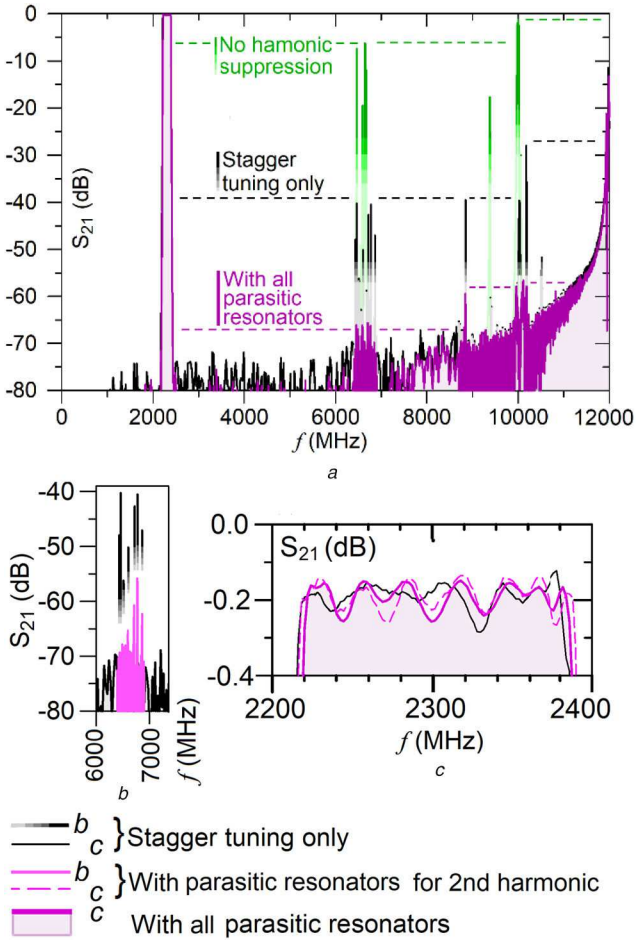

Fig. 8 *Measured filter performance. Response curves: unprocessed data; horizontal dashed lines: stop band envelopes based on curve-fitted or smoothed curves (described in the appendix)*

(a) Filters 1 (stagger tuning only) and 3 (with all harmonic parasitic resonators) compared with no intentional suppression [5], ***(b)*** Filter 2 (2nd harmonic parasitic resonators) compared with filter 1, ***(c)*** Pass band performance of the 3 filters

Table 3 Maximum spurious stop band spurious levels (dB). Data processed as described in the appendix

	Stop band limit, MHz		
Filter no.	8800	10 000	11 400
previous [5]	−6	−6	−1
1	−39	−39	−27
2	−56	−39	−30
3	−67	−58	−57

Table 4 Some microstrip filters with at least 50 dB harmonics attenuation and f_{max}/f_0 (Stop-band limit/passband centre) at least 3.0.

Ref	Suppression Mechanism	Stop-band atten., dB	f_{max}/f_0
this work	combination	67 or 57	3.8 or 4.9
[2]	combination	67	8.8
[35]	periodic capacitance pads	52	4
[34]	coupling at harmonic nodes	50	10
[1]	combination	50	5.6
[36]	resonator overlap	50	3.2

significant error in their amplitude, which is sensitive to small differences in resonant frequencies between the main and parasitic resonators, illustrated in Fig. 4. For filter 2, the simulated 2nd harmonic level is −66 dB, and the measured one, visible in Fig. 8*b* without magnification, is −56 dB. Although it shows that the filters should be designed with a large error margin, the suppression level is excellent.

Spurious responses in superconducting microwave filters have been suppressed, giving in one case response levels of −67 and −57 dB for the second order and third order resonances. The additional pass band loss was too small to be measured, and no additional processing was involved, except perhaps a more complex circuit to be visually inspected.

7 Conclusion

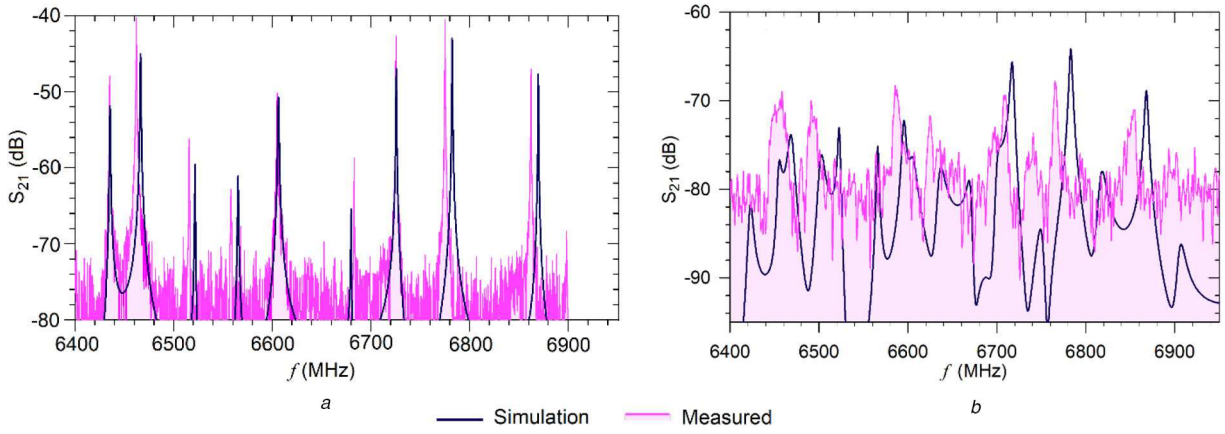

Fig. 9 *Simulated and measured responses near the 2nd harmonic*
(a) Filter 1 (measured data is unprocessed), ***(b)*** Filter 3 (measured data smoothed as described in the appendix)

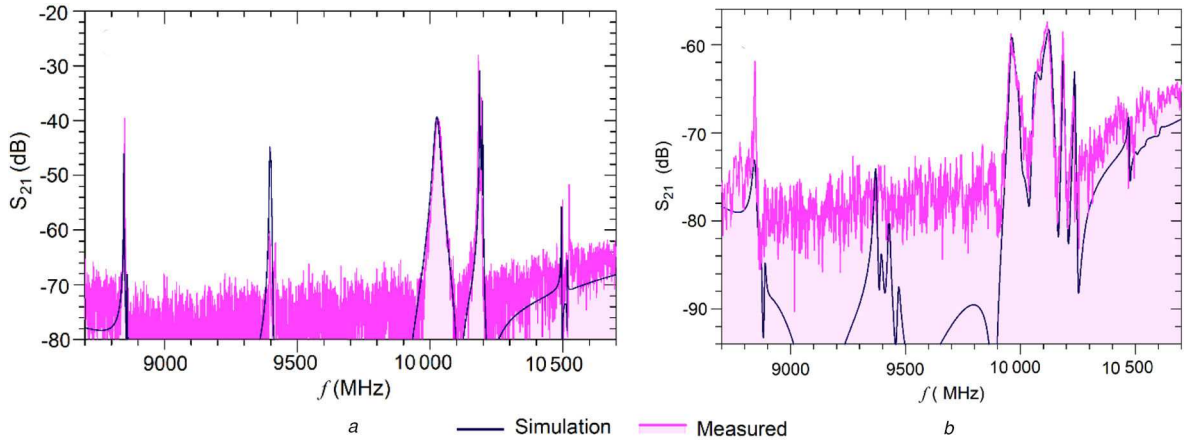

Fig. 10 *Simulated and measured responses near the 3nd harmonic*
(a) Filter 1 (measured data is unprocessed), ***(b)*** Filter 3 (measured data smoothed as described in the appendix)

8 Acknowledgment

The authors are grateful to Anthony Page (University of Birmingham, UK) and Luca Cresci (Acetri Astrophysical Observatory, (INAF), Italy) for able technical assistance, together with Adrian Porch (University of Cardiff, UK) and Robert Semerad (Ceraco Ceramic Coatings GmbH, Ismaning, Germany) for advice on material properties.

9 References

[1] Huang, F.: 'Suppression of harmonics in microstrip filters using a combination of techniques', *IEEE Trans. Microw. Theory Technol.*, 2015, **63**, (10), pp. 3453–3461
[2] Huang, F.: 'Microstrip band-pass filter with −67 dB stop band up to 8.8 times the pass-band center frequency', *Int. J. Microw. Wirel. Technol.*, 2017, **9**, (10), pp. 1937–1944
[3] Huang, F.: 'Suppression of spurious responses in microstrip half-wavelength filters combining stagger tuning and resistive attenuation', *Microw. Opt. Technol. Lett.*, 2016, **58**, (8), pp. 1955–1957
[4] Huang, F.: 'Suppression of harmonics in microstrip filters with stagger tuning and voltage redistributions', *IEEE Trans. Microw. Theory Techn.*, 2014, **62**, (3), pp. 464–471
[5] Huang, F., Bolli, P., Cresci, L., *et al.*: 'Superconducting spiral bandpass filter designed by a Pseudo-Fourier technique', *IET Microw., Antennas Propag.*, 2018, **12**, (8), pp. 1293–1301
[6] Kim, P., Chaudhary, G., Jeong, Y.: 'Wide-stopband and high selectivity step impedance resonator bandpass filter using T-network and antiparallel coupled line', *IET Microw., Antennas Propag.*, 2019, **13**, (11), pp. 1916–1920
[7] Lin, S.-C., Deng, P.-H., Lin, Y.-S, *et al.*: 'Wide-stopband microstrip bandpass filters using dissimilar quarter-wavelength step-impedance resonators', *IEEE Trans. Microw. Theory Techn.*, 2006, **54**, (3), pp. 1011–1018
[8] Jun, S., Chang, K.: 'Second harmonic suppression bandpass filter using nonuniform open stubs', *Microw. Opt. Technol. Lett.*, 2013, **55**, (7), pp. 1451–1453
[9] Hsu, K.-W., Tsou, M.-J., Tseng, Y.-H;, *et al.*: 'Wide-stopband bandpass filter with symmetrical loaded-stub resonators'. Proc. Asia-Pacific Microw. Conf., Melbourne, Australia, December 2011, pp. 1043–1046
[10] Makimoto, M., Yamashita, S.: 'Half-wavelength-type SIR', in: *'Microwave resonators and filters for wireless communications'* (Springer Verlag, Berlin, 2001), pp. 66–83, ISBN 9783642087004
[11] Deng, P-H, Lin, S-C, Lin, Y-S, *et al.*: 'Microstrip bandpass filters with dissimilar resonators for suppression of spurious responses'. 2005 European microwave Conf. proc., Paris, France, October 2005, pp. 1263–1266
[12] Majidifar, S., Al-din Makki, S.V., Ahmadi, A., *et al.*: 'Compact microstrip lowpass filter using stepped impedance spiral resonator'. Fourth int. Conf. on computational intelligence and communication networks, Mathura, India, November 2012, pp. 23–26
[13] 'Tuned mass damper'. Available at https://en.wikipedia.org/wiki/Tuned_mass_damper, accessed Jun 2020
[14] Huang, F.: 'Suppression of superconducting filter spurious response using lossy parasitic resonators', *IET Microw., Antennas Propag.*, 2010, **4**, (12), pp. 2042–2049
[15] Wang, L-M, Chiou, S.M., Chu, M. L., *et al.*: 'Cross-coupled YBCO filters with spurious suppression using tap-connection technique and skew-symmetric feeds', *IEEE Trans. Appl. Supercond.*, 2007, **17**, (20), pp. 894–897
[16] Bilotti, F., Toscano, A., Vegni, L.: 'Design of spiral and multiple split-ring resonators for the realization of miniaturized metamaterial samples', *IEEE Trans. Antennas Propag.*, 2007, **55**, (8), pp. 2258–2267
[17] 'Sonnet'. Available at http://www.sonnetsoftware.com/
[18] Haynes, W.M., Lide, D.R., Bruno, T.J.: '*CRC handbook of chemistry and physics*' (CRC Press, London, 2016, 97th edn.)
[19] Millo, O., Asulin, I., Sharoni, A., *et al.*: 'The superconductor proximity effect in Au-YBa2CuO7-d bilayer films: the role of order parameter anisotropy', *Microelectron. J.*, 2005, **36**, pp. 539–542
[20] Pan, V.M., Tarasov, V.F., Popov, A.G., *et al.*: 'Observation of proximity effect in YBCO/Au bilayer films by microwave surface resistance measurements', *Physica B*, 2000, **284**, (1), pp. 915–916
[21] Pippard, A.B.: 'The surface impedance of superconductors and normal metals at high frequencies II: the anomalous skin effect in normal metals', *Proc. Royal Soc. London Series A, Math. Phys. Sci.*, 1947, **191**, (1026), pp. 385–399
[22] Casimir, H.B.G., Ubbink, J.: 'The skin effect: II. The skin effect at high frequencies', *Philips Tech. Rev.*, 1967, **28**, (10), pp. 300–315
[23] Lancaster, M.J.: '*Passive microwave device applications of high-temperature superconductors*' (Cambridge University Press, Cambridge, UK, 1997)
[24] Porch, A.: private communication
[25] Prozorov, R, Giannetta, R.W., Carrington, A, *et al.*: 'Measurements of the absolute value of the penetration depth in high-Tc superconductors using a low-Tc superconductive coating', *Appl. Phys. Lett.*, 2000, **77**, (25), pp. 4202–4204

[26] Booth, J.C., Holloway, C.L.: 'Conductor loss in superconducting planar structures: calculations and measurements', *IEEE Trans. Microw. Theory Techn.*, 1999, **47**, (6), pp. 769–774
[27] Huang, F.: 'Re-adjustments for MOM calculations of microstrip and stripline power dissipation', *Int. J. Microw. Wirel. Technol.*, accepted for publication, 2020, pp. 1–11, doi: S1759078720000975
[28] Weber, C.: 'Coplanar transmission lines with meandering centre conductors in Y-Ba-Cu-O/Au bilayers', *Supercond. Sci. Technol.*, 1999, **12**, pp. 998–1000
[29] Tarasov, V.F., Korotash, I.V.: 'Band-pass filters for 1.8 GHz frequency range using double-sided YBCO/Au films on CeO2-buffered sapphire', *J. Supercond.*, 2001, **14**, (1), pp. 115–125
[30] Zaitsev, A.G., Schneider, R., Geerk, J., *et al.*: 'Effective microwave surface resistance of gold-contacted YBa2Cu3O7-x thin films', *Appl. Phys. Lett.*, 1999, **75**, pp. 4165–4167
[31] Raihan, K.F., Alvarez, R., Costa, J., *et al.*: 'Highly selective HTS band pass filter with multiple resonator cross-couplings'. 2000 IEEE Microwave Symp. Digest, Boston, USA, 2000, pp. 661–664
[32] Tao, L., Wei, B., Guo, X., *et al.*: 'Miniaturised ultra-narrowband superconducting microstrip filter with stable coupling using optimized twin spiral-in-spiral-out resonators', *IEEE Trans. Appl. Supercond.*, 2019, **29**, (6), pp. 1–7
[33] Huang, F.: 'Ultra-compact superconducting narrowband filters using single and twin-spiral resonators', *IEEE Trans. Microw. Theory Techn.*, 2003, **51**, (2), pp. 487–491
[34] Vladimirov, V.M., Markov, V.V., Shepov, V.N.: 'Microstrip filter with suppression of spurious-bands'. 10th int. Conf. of telecommunications in modern satellite cable and broadcasting services, Nis, Serbia, 2011, pp. 401–403
[35] Orellana, M., Selga, J., Velez, P., *et al.*: 'Design of capacitively loaded coupled-line bandpass filters with compact size and spurious suppression', *IEEE Trans. Microw. Theory Techn.*, 2017, **68**, (4), pp. 1235–1248
[36] Cheong, P., Fok, S.-W., Tam, K.-W.: 'Miniaturized parallel coupled-line bandpass filter with spurious-response suppression', *IEEE Trans. Microw. Theory Techn.*, 2005, **53**, (5), pp. 1810–1816

10 Appendix

Extraction of resonance amplitudes and Q-factors

In filter 1 and in the third harmonics in filter 2, the resonance bandwidths were smaller than expected, and similar to the frequency step in the measurements, as in Fig. 11*a*. Far away from the resonance f_0, the lossy and the hypothetical lossless (infinite Q) cases approximately coincide, and furthermore the width halves for each 6 dB increase in S_{21}, so the lossless curve (black) can be sketched, either on paper or using a software equivalent, together with the centre line, giving f_0. If the highest measured value (purple dot A) is close to f_0, this is a good estimate of the maximum. Further from f_0, as with point B, a correction

$$\Delta L(\text{dB}) = -10\log\left[1-\left(\frac{\Delta f}{\Delta f_\infty}\right)^2\right] \tag{2}$$

can be calculated from the normalised Lorentzian curve $S_{21} = 1/|1 + \text{j}f|$ compared with the lossless $S_{21} = 1/|f|$. Compared with full curve fitting, a few examples with the current data suggests an accuracy of about 1 dB for $\Delta L(\text{dB}) < 3$ dB from a visual estimate of $\Delta f/\Delta f_\infty$.

Meanwhile, weak signals as in Filter 3 (Fig. 11*b*) are subject to noise-like measurement error. Because of the wider bandwidths

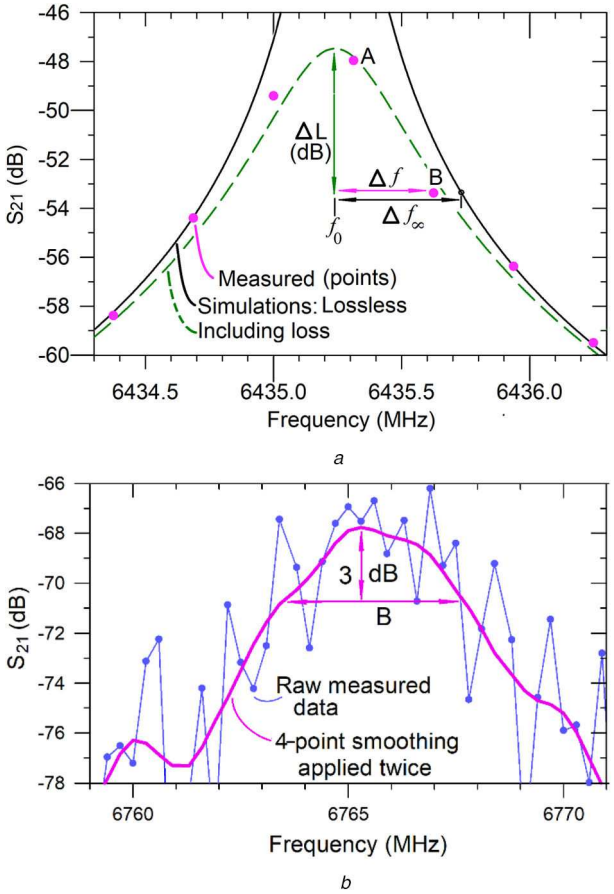

Fig. 11 *Resonance amplitudes and Q-factors*
(a) Only just sufficient sampling, ***(b)*** With large measurement scatter

(typically 5 MHz), smoothing can be employed. A wide smoothing interval also distorts the wanted signal, so a compromise is required. For the present work, 4-point smoothing is applied twice. Perhaps it is better described as three points and two halves; in each run,

$$4s_n = 0.5S_{n-2} + S_{n-1} + S_n + S_{n+1} + 0.5S_{n+2} \tag{3}$$

where S_{n-2} …S_{n+2} are consecutive values of S_{21} (in dB) and s_n is the running mean. The peak is reduced typically by 0.3 dB. For the 2nd harmonics of filter 2, with peaks of 50–60 dB, there was less measurement scatter; this could be smoothed manually on graph paper.

In Section 3, the frequency step for the single resonances and the noise were both much smaller, so the smoothing might have been superfluous. The 3 dB bandwidth was taken and R_s was found by adjusting its value in a simulation until the same bandwidth was obtained, or the whole curve was visually matched.